HHS Public Access

Author manuscript

J Immunol. Author manuscript; available in PMC 2020 October 15.

Published in final edited form as:

J Immunol. 2019 October 15; 203(8): 2328–2338. doi:10.4049/jimmunol.1801604.

T CELL SPECIFIC ADAPTOR PROTEIN REGULATES MITOCHONDRIAL FUNCTION AND CD4+ T REGULATORY CELL ACTIVITY *IN VIVO* FOLLOWING TRANSPLANTATION

Johannes Wedel[*,†,‡], **Maria P. Stack**[*,†,‡], **Tatsuichiro Seto**[*,†,‡], **Matthew M. Sheehan**[*,†], **Evelyn A. Flynn**[*,†,‡], **Isaac E. Stillman**[§,¶], **Sek Won Kong**[‡,‖], **Kaifeng Liu**[*,†,‡,#], **David M. Briscoe**[*,†,‡]

[*]Transplant Research Program, Boston Children's Hospital, Boston MA, USA

[†]Division of Nephrology, Department of Pediatrics, Boston Children's Hospital, Boston, MA, USA

[‡]Department of Pediatrics, Harvard Medical School, Boston, MA, USA

[§]The Department of Pathology, Beth Israel Deaconess Medical Center, Boston, MA, USA

[¶]Department of Pathology, Harvard Medical School, Boston, MA, USA

[‖]Computational Health Informatics Program, Boston Children's Hospital, Boston MA, USA

[#]Division of Pulmonary Diseases, Department of Medicine, Boston Children's Hospital, Boston, MA, USA

Abstract

T cell specific adaptor protein (TSAd, encoded by the *SH2D2A* gene) is an intracellular molecule that binds Lck to elicit signals that result in cytokine production in $CD4^+$ Teff cells. Nevertheless, using S*h2d2a* knockout mice (TSAd KO), we find that alloimmune $CD4^+$ Teff responses are fully competent in the absence of TSAd *in vivo*. Furthermore, and contrary to expectations, we find that allograft rejection is accelerated in KO recipients of MHC class II mismatched B6.C-H-2^{bm12} heart transplants *vs.* WT recipients. Also, KO recipients of fully MHC mismatched cardiac allografts are resistant to the graft prolonging effects of costimulatory blockade. Using adoptive transfer models, we find that TSAd KO Tregs are less efficient to suppress Teff function and they produce IFN-γ following mitogenic activation. In addition, pyrosequencing demonstrated higher levels of methylation of CpG regions within the TSDR of KO *vs.* WT Tregs, suggesting that TSAd in part promotes Treg stability. By Western blot, Lck is absent in the mitochondria of KO Tregs, and ROS production by mitochondria is reduced in KO *vs.* WT Tregs. Full transcriptomic sequencing demonstrated that the key mechanism of TSAd function in Tregs relates to its effects on cellular activation, rather than intrinsic effects on mitochondria/metabolism. Nevertheless, KO Tregs compensate for a lack of activation by increasing the number of mitochondria per cell. Thus,

Correspondence to: David M. Briscoe, M.D., Transplant Research Program and the Division of Nephrology, Boston Children's Hospital, 300 Longwood Ave., Boston, MA 02115, USA. Phone: +1 (617) 919-2992 Fax: +1 (617) 730-0130. david.briscoe@childrens.harvard.edu.

Conflicts of Interest

Potential conflicts of interest have been reviewed by the Office of General Counsel at Boston Children's Hospital. The authors of this manuscript declare no conflicts of interest.

TSAd serves as a critical cell intrinsic molecule in $CD4^+Foxp3^+$ Tregs to regulate the translocation of Lck to mitochondria, cellular activation responses and the development of immunoregulation following solid organ transplantation.

Introduction

T-cell-specific Adaptor Protein (TSAd, encoded by the *SH2D2A* gene) is an SH2 domain containing intracellular adaptor molecule that activates the protein tyrosine kinase Lck and elicits intracellular signals resulting in cytokine production (1-3). As its name suggests, TSAd was initially identified based on its expression in T cells (1, 3-6), but more recent studies have demonstrated its expression and function in other cell types (6-8). Nevertheless, targeted disruption of the TSAd gene in mice does not cause any major developmental abnormalities and is rather associated with defects in immune function (3, 9, 10), indicating that its primary function is indeed linked to T cell biology. Furthermore, genetic polymorphisms in the *SH2D2A* gene in humans result in lower TSAd protein expression levels and have been associated with the development of multiple sclerosis and juvenile rheumatoid arthritis (2, 11-13). These collective observations are most suggestive that TSAd plays a major role in immunity and notably in human autoimmune disease. However, the cell intrinsic function of TSAd in regulatory T cells (Tregs) is not known, and its role in the modulation of effector T cell (Teff) activation *in vivo* has not been reported.

Mechanistically, TSAd is reported to augment upstream T cell receptor (TCR)-dependent signaling through an interaction that results in the amplification of Lck phosphorylation and Lck-dependent responses (4, 14). TSAd also functions to augment synapse formation between $CD4^+$ T cells and APCs (10), and it enhances CD28-dependent costimulation (15). In this manner, TSAd decreases the threshold signal required for antigen-dependent activation of $CD4^+$ T cell subsets. In addition, it has been reported to function in T cell migration, notably in response to the chemokines SDF-1α and RANTES (5, 16, 17). However, knockout of the *Sh2d2a* gene in mice is not associated with immunodeficiency, but rather results in susceptibility for autoimmunity (3, 9). Current models suggest that Treg dysfunction in $Sh2d2a^{-/-}$ mice (also called $TSAd^{-/-}$ mice) is due to a deficiency in IL-2 production by Teffs, and thus, IL-2-dependent survival and activity of $CD4^+Foxp3^+$ Tregs (9). However, the autoimmune disease previously reported in $TSAd^{-/-}$ mice is different from that reported in $Il2^{-/-}$ or $Il2r^{-/-}$ mice (18-20), and recent studies are suggestive that TSAd may have a cell intrinsic function in Tregs (21). Since mutations in *SH2D2A* are relatively common in humans (11-13), these observations indicate that its biology has broad implications in Treg-associated disease(s).

In this study, we wished to determine the relative function of TSAd in Teffs and Tregs *in vivo* and the development of immunoregulation following transplantation. Contrary to expectations, we find that allopriming and Teff cell responses are sustained in $TSAd^{-/-}$ recipients of cardiac transplants. Furthermore, we find that KO recipients have accelerated graft failure following MHC class II mismatched transplantation, and they are resistant to the graft prolonging effects of costimulatory blockade. Mechanistically, we find that $TSAd^{-/-}$ Tregs are less efficient to suppress Teff responses and they possess effector function as

evidenced by IFN-γ production. Untargeted transcriptomic RNA-sequencing indicates that the major function of TSAd in Tregs relates to its effects on cellular activation, suggesting that it is potent to modulate $CD4^+Foxp3^+$ Treg biology through cell intrinsic mechanisms. We also find that mitochondria in $TSAd^{-/-}$ Tregs lack Lck, and have reduced ROS production/activation. However, $TSAd^{-/-}$ Tregs compensate by increasing the numbers of mitochondria/cell and this effect is not associated with altered Treg metabolism. These collective findings have broad implications, and suggest that mutations in the *SH2D2A* gene in humans will results in generalized $CD4^+Foxp3^+$ Treg dysfunction and susceptibility to graft loss following solid organ transplantation and chronic inflammatory/autoimmune disease(s).

Materials and Methods

Mice

Male 6-8 week old C57BL/6 ($H\text{-}2^b$), B6.C-$H\text{-}2^{bm12}$ and BALB/c ($H\text{-}2^d$) mice were purchased from the Jackson Laboratory (Bar Harbor, ME). *Sh2d2a*$^{-/-}$ knockout mice ($TSAd^{-/-}$; also called RIBP and TSAd knockouts) were generated by Jeffrey A. Bluestone (University of California, San Francisco, CA (3)) and gifted to the laboratory by Philip King (University of Michigan, Ann Arbor, MI (9)). The mice have been backcrossed onto the C57BL/6 ($H\text{-}2^b$) background.

Cardiac Transplantation

Intra-abdominal heterotopic heart transplantation was performed as previously described (22, 23), and graft survival was monitored by palpation of the heartbeat. In some experiments, BrdU (1 mg; Biolegend, San Diego, CA) was injected intraperitoneally every 12 hours for 72 hours into recipients, and BrdU incorporation in $CD4^+$ T cell subsets was analyzed by flow cytometry using the BD BrdU Flow Kit (BD Pharmingen, San Jose, CA). Anti-mouse CD40L antibody (anti-CD154, clone MR-1), recombinant CTLA4-Ig or control-Ig (clone human Fc-G1) were administered on days 0, 2 and 4 post-transplantation (200 μg/day; all BioXcell, West Lebanon, NH). All studies were performed according to an approved Institutional Animal Care and Use Committee protocol at Boston Children's Hospital.

Immunohistochemistry

Following harvest, allografts were divided and either frozen in liquid nitrogen in OCT or fixed in 10% formaldehyde in PBS (Fisher Scientific, Kalamazoo, MI) overnight at 4°C. Formalin fixed tissue was paraffin-embedded, sectioned (~3 μm thick) and mounted on poly-l-lysine coated slides (Thermo Fisher, Tewksbuy, MA). The slides were deparaffinized, rehydrated and stained with Harris haematoxylin and eosin (all Thermo Fisher, Tewksbuy, MA). Frozen tissue was cryosectioned (~4 μm thick), fixed in acetone for 10 minutes, quenched with 0.3% hydrogen peroxide in PBS for 30 minutes, blocked for 30 minutes with 2% bovine serum albumin (BSA) in PBS and incubated with primary antibody (diluted in 2% BSA/PBS) overnight at 4°C. After a wash in 0.5% Tween 20 in PBS, sections were incubated with a species-specific peroxidase-labeled secondary antibody (Jackson ImmunoResearch, West Grove, PA) for 1 hour at room temperature. The slides were washed three times and peroxidase-activity was developed using 0.05% 3-amino-9-ethyl-carbazole

and 0.015% hydrogen peroxide in 0.05 M acetate buffer pH 5.5. Finally, each slide was counterstained in Gill's haematoxylin (Sigma-Aldrich, St. Louis, MO) and mounted in glycerol gelatin (Thermo Fisher, Tewksbuy, MA). Images were evaluated on a Nikon Eclipse 80i (Nikon, Mississauga, Ontario, Canada) using a Retiga-2000R CCD camera (QImaging, Surrey, Canada) equipped with NIS Elements software (version 3.22.15; Nikon, Melville, NY). Infiltrates were evaluated by standard grid counting at 40x high power field magnification of 12 different fields/slide by 3 independent investigators. Data was expressed as the mean infiltration per allograft.

Isolation and culture of murine T cells and T cell subsets

Murine T cell subsets were isolated from splenocytes using the EasySep mouse $CD4^+$, naive $CD4^+$ and $CD4^+CD25^+$ T Cell Isolation Kits (Stemcell Technologies, Vancouver, Canada) or FACS-sorted using an Aria IIU FACS-sorter (BD Biosciences, San Diego, CA). Purity was consistently above 95% for bead isolated cells and up to 98% for FACS-sorted cells (Supplemental Figure 1). Graft infiltrating cells were isolated by enzymatic (1 mg/mL collagenase I; Worthington, Lakewood, NJ) and mechanical disruption, and subsequently enriched over a 67-44% Ficoll density gradient. Isolated $CD4^+$ T cells were cultured in RPMI 1640 (Lonza, Walkersville, MD) supplemented with 10% FBS (Sigma-Aldrich, St. Louis, MO), 2 mM L-glutamine, 1 mM sodium pyruvate, 0.75 g/L sodium bicarbonate, 100 U/mL penicillin/streptomycin, 0.1 mM non-essential amino acids (all Lonza, Walkersville, MD) and 50 μM 2-mercaptoethanol (Sigma-Aldrich, St. Louis, MO). The cells were stimulated with plate-bound anti-CD3 (clone 145-2C11, BioXcell, West Lebanon, NH) in the absence or presence of soluble anti-CD28 (clone 37.51, Biolegend, San Diego, CA), and cytokines were evaluated as indicated by each experiment. *In vitro* differentiation of $CD4^+$ Treg cells was performed by culturing naive $CD4^+CD25^-$ cells for 2 days with plate-bound anti-CD3 (2 μg/mL), anti-CD28 (1 μg/mL), anti-IL-4 (500 ng/mL, clone 11B11), anti-IFN-γ (2 μg/mL, clone XMG1.2), murine TGF-β1 (5 ng/mL), murine IL-2 (50 U/mL) (all Biolegend, San Diego, CA) and 10 nM rapamycin (Wyeth-Ayerst, Philadelphia, PA) or 100 nM all-trans retinoic acid (Sigma-Aldrich, St. Louis, MO) in DMEM (Lonza, Walkersville, MD) supplemented with 10% fetal bovine serum (Sigma-Aldrich, St. Louis, MO), 2 mM L-glutamine, 1 mM sodium pyruvate, 0.75 g/L sodium bicarbonate, 100 U/mL penicillin/streptomycin, 0.1 mM non-essential amino acids (all Lonza, Walkersville, MD) and 50 μM 2-mercaptoethanol (Sigma-Aldrich, St. Louis, MO). On day 2, the cells were transferred to a new cell culture plate in medium supplemented with 50 U/mL IL-2 in the absence of anti-CD3 for an additional 2 days after which the efficiency of iTreg generation was evaluated by CD25 and Foxp3 expression.

Proliferation assays

T cell proliferation was assessed by the addition of 1 μCi of ^{3}H-thymidine/well (Perkin Elmer, Boston, MA) during the last 16 hours of culture. Incorporated ^{3}H-thymidine was assessed in a Wallac 1450 MicroBeta TriLux scintillation counter (Perkin Elmer, Boston, MA).

ELISPOT assays

$CD4^+$ T cells (3×10^4) were cultured in 96-well polyvinylidene fluoride plates (Immobilon-P, Millipore, Billerica, MA) and stimulated with irradiated (1700 rad) splenocytes and/or with anti-CD3/anti-CD28-coated beads (1:1 ratio beads:cell; Life Technologies, Carlsbad, CA) for 24 hours. Subsequently, the cells were stained according to the ELISPOT manufacturers protocol (eBioscience and BD Biosciences, San Diego, CA). After staining, the plates were scanned and analyzed on an ImmunoSpot S6 Ultra ELISpot reader (version 5.0, CTL, Shaker Heights, OH).

Cytosolic, mitochondrial and nuclear protein isolation and Western blot analysis

Nuclear extracts were prepared by lysing cells in hypotonic buffer containing 10 mM HEPES, 10 mM potassium chloride, 1.5 mM magnesium chloride, 1 mM EDTA, 500 μM DTT, and 200 μM PMSF (all Sigma-Aldrich, St. Louis, MO) supplemented with protease and phosphatase inhibitors (Thermo Scientific, Tewksbuy, MA) for 15 minutes on ice. After the addition of 1% IGEPAL, the cells were vortexed and cytosolic and nuclear fractions were separated by centrifugation. Nuclei were resuspended in 20 mM HEPES, 25% glycerol, 4.2 mM sodium chloride, 1.5 mM magnesium chloride, 200 μM EDTA, 0.5 μM DTT, 200 μM PMSF (all Sigma-Aldrich, St. Louis, MO) and protease and phosphatase inhibitors (Thermo Scientific, Tewksbuy, MA) for 20 minutes on ice; subsequently, DNA was removed by centrifugation. Mitochondrial proteins were isolated using the AMRESCO mitochondrial protein isolation buffer (VWR, Radnor, PA) supplemented with protease and phosphatase inhibitors (Thermo Scientific, Tewksbuy, MA). Samples were subjected to electrophoresis on 4-15% gradient SDS-polyacrylamide gels (Bio-Rad, Hercules, CA) and separated proteins were transferred to PVDF membranes (Milipore, Billerica, MA). Membranes were blocked in TBS containing 0.1% Tween 20 and 5% BSA (Fisher Scientific, Kalamazoo, MI) for 1 hour, and incubated with primary antibodies overnight at 4°C. Membranes were subsequently washed and incubated with species-specific peroxidase-labeled secondary antibodies (Jackson ImmunoResearch, West Grove, PA) for 1 hour at room temperature. After washing, the protein of interest was visualized by chemiluminescence (Thermo Scientific, Tewksbuy, MA) in a ChemiDoc MP imaging system (Bio-Rad, Hercules, CA). The membranes were stripped (Thermo Scientific, Tewksbuy, MA) and reprobed with antibodies to evaluate protein loading.

Multi-analyte profiling of Treg cytokine production

Cell culture supernatants were profiled using the mouse cytokine/chemokine 25 plex magnetic bead panel (Milipore, Billerica, MA) on a Luminex LX200 platform equipped with xPonent software (version 3.1.871.0; Luminex, Austin, TX).

Flow cytometric analysis

Cells were incubated with conjugated monoclonal antibodies diluted in 0.5% BSA in PBS for 30 minutes at 4°C, washed and fixed with 4% paraformaldehyde. Foxp3 expression was evaluated by fixing and permeabilizing cells using a buffer set prior to staining using an anti-Foxp3 mAb (clone FJK-16s), or isotype (eBR2a) as a control, according to the manufacturer's instructions (all eBioscience, San Diego, CA). IRF-4 (clone IRF4.3E4),

Helios (clone 22F6), EOS (clone ESB7C2, eBioscience, San Diego, CA) and Blimp-1 (clone 5E7) staining was performed using the True-Nuclear Transcription Factor Buffer set according to supplier's instructions (all Biolegend, San Diego, CA). Cells were analyzed on a FACS Calibur flow cytometer (BD Biosciences, San Diego, CA) within 24 hours of staining and at least 50,000 gated events were collected per sample. Data were analyzed using Flowjo software (version X.0.7, Tree Star, Ashland, OR).

Treg suppression assays

In vitro suppression was performed by co-culture of CFSE-labeled (2 μM; Life Technologies, Carlsbad, CA) $CD4^+CD25^-$ T responder cells with increasing ratios of $CD4^+CD25^{high}$ Tregs or iTregs (generated *in vitro*) and either irradiated (1700 rad) antigen presenting cells or anti-CD3/anti-CD28 coated beads (1:1 ratio beads:responder cell; Life Technologies, Carlsbad, CA). Responder cell activation was analyzed using the standard CFSE-dilution assay, and expansion indices were calculated using the Flowjo's proliferation module (version 9.9.3, Tree Star, Ashland, OR); suppression by knockout cells were normalized to the suppressive function of wild type Tregs, as previously described (24). Normalized suppressive function was plotted against corresponding ratio of Tregs:Tresp. Suppressive function was also evaluated using the IFN-γ ELISPOT assay.

TSDR methylation analysis

TSDR DNA methylation analysis was performed on two male and one female TSAd knock-out mice, and on three age/sex-matched wild type controls. FACS-sorted $CD4^+$ Treg and Teff cells (purity of >99%) were pelleted, frozen and processed for pyrosequencing by EpigenDx (Hopkinton, MA). Briefly, genomic DNA was isolated, bisulfite-modified and the 14 CpG islands within the promoter and intron 1 of the *Foxp3* gene were amplified by PCR and pyrosequenced. Sequences were aligned to the mouse genome and the percentage of converted (unmethylated) cytosine to uracil/thymidine for each CpG site was evaluated. All 14 CpG regions in each sample were analyzed and low DNA methylation in the regions 1-7 was used to indicate a comparable purity between KO and WT cells. Only the male samples are shown as we observed that the inactivated X chromosome remains methylated within the TSDR (maximum of 50% demethylation in female samples).

Transcriptomic analysis

RNA-sequencing library preparations were performed as previously described (25, 26). Total RNA was isolated using MyOne Silane Dynabeads (Thermo Fisher, Tewksbury, MA). RNA was fragmented and barcoded using 8-bp barcodes with standard Illumina adaptors. Libraries were enriched using Agencourt AMPure XP bead cleanup (Beckman Coulter, Brea, CA), PCR amplified, gel purified, and quantified using a Qubit high-sensitivity DNA kit (Thermo Fisher, Tewksbury, MA). Libraries were quality tested using Tapestation high-sensitivity DNA tapes (Agilent Technologies, Santa Clara, CA) and sequenced on a HiSeq 2500 (Illumina, San Diego, CA) using 50-bp single-end reads. Reads were aligned to the mouse reference genome GRCm38.p6 using 2-pass STAR aligner version 2.6.0 (27) and gene expression was quantified using the GENCODE gene models (Release M14) using HTseq-count-method (28). Counts were normalized, and differential gene expression and principle components were calculated using the DESeq2 method (version 1.14.1) in the R

Statistical Computing Environment (version 3.3.2) (29). False discovery rates were calculated and genes with *Padj*<0.001 were considered differential expressed. Gene set enrichment analysis (version 3.0, Broad Institute, Cambridge, MA) was performed using the $\log_2$ ratio of TSAd$^{-/-}$ to WT CD4$^+$CD25^{high} Tregs at each time point and the immunologic gene sets (C7) of the Molecular Signatures Database with defult parameters of GSEA (30).

Quantitative Polymerase Chain Reaction

Total RNA was isolated using the RNeasy isolation kit (Qiagen, Valencia, CA) and reverse-transcribed into cDNA using the qScript Supermix from Quanta Biosciences (Gaitherburg, MD). cDNA was diluted 1:10 in RNase-free water and stored at −20°C until use. qPCR was performed on a 7300 real-time PCR system (Applied Biosystems, Foster City, CA) using 1 μl cDNA, PerfeCTa SYBR green (Quanta Biosciences, Gaitherburg, MD) and individual primers (Table 1) in a final concentration of 5 μM. Samples were run in duplicate and the relative gene expression was determined with the comparative cycle threshold (Ct) method and expressed as $2^{-Ct(\text{target gene})-Ct(GAPDH)}$.

Statistics

Statistical analyses were performed using one-way analysis of variance (ANOVA) or the Student's t-test (Prism, version 5.03, GraphPad, La Jolla, CA) as appropriate. If the equality test failed, the Kruskal-Wallis-test was used. *P*-values less than 0.05 were considered statistically significant. Heatmaps were generated using the heatmap.2 function in the gplots package (version 3.0.1.1).

Results

CD4$^+$ T effector responses are sustained *in vivo* in TSAd knockout mice:

We initially cultured purified populations of CD4$^+$ T cells from wild type (WT) or TSAd$^{-/-}$ mice with anti-CD3/anti-CD28, and we compared proliferative responses as well as IL-2, IL-4 and IFN-γ production by ELISPOT. As illustrated in Figures 1A-C, TSAd$^{-/-}$ CD4$^+$ T cells including both naive CD4$^+$CD25$^-$ as well as CD4$^+$CD25^{high} subsets are hypoproliferative (*P*<0.001) and produce lower levels of cytokines (*P*<0.001) *vs.* WT cells following activation with mitogen. However, increasing the concentration of mitogen and/or the addition of IL-2 into cultures overcomes this threshold effect, and readily induces activation responses in knockout cell subsets (Figure 1B-C). These results confirm previous observations (3, 5, 6, 14) and support a model linking TSAd biology to CD4$^+$ Teff function. However, TSAd$^{-/-}$ mice fail to develop symptoms of immunodeficiency, and the phenotypes of TSAd$^{-/-}$ CD4$^+$ T cells and CD4$^+$Foxp3$^+$ Tregs are similar to WT mice (Supplemental Figure 2), even following exposure to pathogens (data not shown and (6)). Thus, we postulate that these *in vitro* findings may not be of great significance *in vivo*.

To evaluate CD4$^+$ Teff function *in vivo*, we used TSAd$^{-/-}$ mice (H-2^b background) as recipients of fully MHC mismatched BALB/c (H-2^d) donor heart transplants. Contrary to expectations, we found that graft survival was identical in TSAd$^{-/-}$ and WT recipients (Figure 2A). Since this mismatch combination results in the clonal expansion, differentiation

and function of $CD4^+$ Teff cells (31), our findings indicate that TSAd is redundant for alloimmune effector $CD4^+$ T cell activation and acute rejection *in vivo*.

TSAd knockout mice reject cardiac allografts following MHC class II mismatched transplantation:

We next evaluated graft survival following the transplantation of MHC class II mismatched B6.C-H-2^{bm12} donor hearts into either $TSAd^{-/-}$ or WT mice (both H-2^b). In this model, $CD4^+$ Teff cell activation and rejection is more insidious due to the relative expansion and function of $CD4^+$ Tregs (32, 33); as expected, median graft survival was >45 days (Figure 2B). Consistently however, we observed that graft failure was markedly accelerated in $TSAd^{-/-}$ recipients (MST=22 days) *vs.* WT recipients ($P<0.01$, Figure 2B). Two weeks post-transplantation, inflammatory cell infiltrates were markedly increased within allografts harvested from $TSAd^{-/-}$ recipients (Figure 2C-G and data not shown). Also, the mRNA expression of several proinflammatory cytokines including IL-2, IL-4 and TNFα was increased in allografts harvested from $TSAd^{-/-}$ *vs.* WT recipients (Figure 2H). Phenotyping demonstrated expanded numbers of $CD3^+$ T cells, lower numbers of $CD4^+Foxp3^+$ subsets ($P<0.05$) and a higher Teff:Treg ratio ($P<0.01$) in $TSAd^{-/-}$ *vs.* WT recipients (Figure 3A-E and Supplemental Figure 3). On day 18 post-transplantation, there was no difference in the frequency of $CD44^{high}CD62L^{low}$ effector memory Treg (eTreg) subsets or NRP-1^+ Tregs (Figure 3F). However, $TSAd^{-/-}$ Tregs had a trend for lower levels of expression of Helios, EOS and Blimp-1 (Figure 3G) as well as cell surface GITR, CTLA-4 and PD-1 (Figure 3H), suggestive of an overall reduced immunoregulatory phenotype. We also examined the expansion and turnover of Tregs in $TSAd^{-/-}$ transplant recipients using the *in vivo* BrdU incorporation assay, and found no differences *vs.* WT recipients (Figure 3I). In contrast, $TSAd^{-/-}$ Teff cell proliferation was significantly increased (Figure 3I) and allopriming of recipient $CD4^+$ Teff cells was greater in $TSAd^{-/-}$ *vs.* WT recipients (Figure 3J). Collectively, these findings are most suggestive that TSAd is functional in the suppressive activity of $CD4^+Foxp3^+$ Tregs following transplantation.

TSAd knockout recipients of fully MHC mismatched cardiac allografts are resistant to costimulation blockade:

To further determine the effects of TSAd on alloimmune $CD4^+$ T cell responses, we examined the effect of costimulatory blockade on graft survival using either $TSAd^{-/-}$ or WT mice as recipients of fully MHC mismatched BALB/c cardiac allografts (Figure 4A-B). Peri-transplant administration of anti-CD40L (anti-CD154, on days 0, 2 and 4) resulted in prolonged graft survival in WT recipients (MST >40 days) *vs.* untreated or control Ig-treated recipients (MST of 8 days; $P<0.01$, Figure 4A) as previously reported (23, 34). However, anti-CD40L was ineffective to prolong survival in $TSAd^{-/-}$ recipients (MST 19 days, $P<0.01$, Figure 4A) and all grafts failed (n=9) by day 22 post-transplant (Figure 4A). Similarly, CTLA4-Ig treatment prolonged graft survival in WT recipients (MST >40 days; Figure 4B), but was ineffective in $TSAd^{-/-}$ recipient mice (MST 10 days; $P<0.05$).

Our collective findings indicate that $CD4^+$ Treg activity is reduced in $TSAd^{-/-}$ mice resulting in a failure to suppress allopriming and graft rejection *in vivo*. To confirm this interpretation, we transplanted fully MHC mismatched BALB/c hearts into C57BL/6

Rag2$^{-/-}$ *Il2rg*$^{-/-}$ recipients, and adoptively transferred either TSAd$^{-/-}$ or WT Tregs on day 2 post-transplantation. On day 18 post-transplantation, recipient mice received CD4^{+}CD25^{-} Teff cells to challenge Treg-based immunoregulation. In control mice (without Treg transfer on day 2), we find that day 18 transfer of WT Teffs elicits graft failure within 16 days post-transfer. In contrast, transfer into mice that received WT Tregs (on day 2) resulted in a prolongation of graft survival to a median of 50 days post-transfer (Figure 4C). However, graft survival was not as prolonged when TSAd$^{-/-}$ Tregs were used in the initial day 2 adoptive transfer (MST=30 days; P<0.05 *vs.* WT Tregs, Figure 4C). These findings further indicate that TSAd modulates CD4^{+}Foxp3^{+} Tregs cell activity and/or stability *in vivo*.

CD4^{+}Foxp3^{+} Tregs from TSAd knockout mice have attenuated activation responses and possess pro-inflammatory effector function:

To understand the molecular basis for the function of TSAd, we performed untargeted transcriptomic profiling of FACS-sorted and mitogen-activated TSAd$^{-/-}$ and WT CD4^{+}CD25^{high} Tregs using RNA-sequencing (Figure 5A-D). We find that TSAd regulates (*Padj*<0.001) the expression of only few genes in resting Tregs (no anti-CD3 stimulation; Supplemental Figure 4A). Furthermore, while WT Tregs respond to anti-CD3 stimulation with the differential expression of >300 genes (Supplemental Figure 4B), anti-CD3-activated TSAd$^{-/-}$ Tregs have a minimal response, with the differential expression of only 4 genes (Supplemental Figure 4B). Principal component analyses of WT transcriptomes showed activation-induced changes (Figure 5B). In contrast, TSAd$^{-/-}$ transcriptomes did not respond to mitogen activation (Figure 5B). Gene set enrichment analysis comparing activated TSAd$^{-/-}$ to WT transcriptomes showed a high normalized enrichment score (NES) for genes expressed in resting *vs.* activated Tregs (Figure 5C). Independent of their activation status, we also noted that TSAd$^{-/-}$ Treg transcriptomes were enriched for genes that are higher expressed in Teff cells *vs.* Tregs (Figure 5D and Supplemental Figure 4C), suggesting that TSAd$^{-/-}$ Tregs have potential to be unstable and/or possess effector function. Collectively, untargeted transcriptomic analysis indicates that TSAd$^{-/-}$ Tregs are generally unresponsive to anti-CD3 stimulation, further supporting a critical role for TCR/TSAd-induced signaling in active immunoregulation and/or in the Treg phenotype.

To next evaluate the effect of TSAd on CD4^{+} Treg stability, we performed DNA methylation assays of CpG motifs within the Treg-specific demethylated region (TSDR) of the *Foxp3* gene. CD4^{+}Foxp3^{+} Tregs were FACS-sorted from the spleens of WT or TSAd$^{-/-}$ mice, DNA was isolated and methylation was analyzed as we described (23). In contrast to WT Tregs which are heavily demethylated, pyrosequencing demonstrated increased methylation of CpG regions 9-14 of the TSDR in TSAd$^{-/-}$ Tregs (Figure 5E and Supplemental Figure 4D). This observation is further suggestive that TSAd$^{-/-}$ Tregs are not fully activated and/or may lack suppressive function. In standard *in vitro* suppression assays (using purified FACS-sorted populations of WT or TSAd$^{-/-}$ Tregs) we find no major difference in the percent inhibition of WT CD4^{+}CD25^{-} responder proliferation by each Treg population (Figure 5F-G). However, TSAd$^{-/-}$ Tregs produced high levels of IFN-γ; also, in suppression assays IFN-γ production was not inhibited (Figure 5H). Furthermore, purified populations of CD4^{+}CD25^{high} Tregs, isolated from the spleens of TSAd$^{-/-}$ mice produced significantly higher levels of IFN-γ (P<0.01) and there was a trend for higher secretion of IL-17 in TSAd

$^{-/-}$ as compared to WT Treg cells (Supplemental Figure 4E). Finally, we evaluated the effect of TSAd on Treg expansion and differentiation by culturing naive TSAd$^{-/-}$ CD4^{+} T cells in iTreg-inducing conditions *in vitro*. As illustrated in Supplemental Figure 4F (and data not shown), we find that TSAd$^{-/-}$ iTregs (CD4^{+}CD25^{high}Foxp3^{+} cells) expand in a similar manner as that observed using WT cells. Collectively, these observations are suggestive that TSAd promotes activation responses within CD4^{+} Treg subsets and that knockout cells have potential to dedifferentiate and/or to possess effector function.

TSAd regulates mitochondrial Lck activity as well as mitochondrial mass in CD4^{+} Tregs:

By Western blot analysis, we find that TSAd is expressed in the cytosol, but not within the mitochondria of Tregs (Figure 6A). We also find that Lck is expressed in both the cytosol and the mitochondria of WT CD4^{+}CD25^{high} Tregs (Figure 6B), but is notably lacking on the mitochondria of TSAd$^{-/-}$ Treg cells (Figure 6B). Since the Lck kinase is reported to be functional within the mitochondria of CD4^{+} T cells (35), we assessed depolarization of mitochondria following treatment with anti-CD3 and find that it is markedly absent in TSAd $^{-/-}$ *vs.* WT cells (Figure 6C). We also used a reactive oxygen species (ROS)-sensitive probe (CM-H_2DCFDA) to evaluate function and find that activation-induced ROS production is lacking in mitochondria from TSAd$^{-/-}$ Tregs following stimulation (Figure 6D). These findings indicate that TSAd is associated with mitochondrial Lck activity and is functional in mitochondrial activation/depolarization within Tregs.

We next isolated CD4^{+}CD25^{high} Tregs from WT and TSAd$^{-/-}$ mice, and metabolism was compared using extracellular flux assays in a Seahorse XFe96 bioanalyzer. The measurement of glycolytic activity (as assessed by the extracellular acidification rate, ECAR, Figure 6E left panel), was identical in each cell type. Also, oxidative phosphorylation, as measured by the oxygen consumption rate (OCR), was identical at basal levels as well as under maximal stress (Figure 6E right panel). Thus, it is likely that TSAd functions to shuttle/translocate cytosolic Lck to mitochondria, and in its absence, mitochondrial Lck-dependent events are deficient.

Since Lck-dependent events also regulate mitochondrial morphology (35), we finally performed electron microscopy on WT and TSAd$^{-/-}$ Tregs. As illustrated in Figure 6F, we find a prominent increase in the number of mitochondria per TSAd$^{-/-}$ cell (Figure 6F; $P<0.0001$ *vs.* WT Treg cells), but there was no demonstrable difference in morphology. We also used MitoTracker Green uptake and qPCR to confirm the significant increase in mitochondrial mass in TSAd$^{-/-}$ Tregs *vs.* WT cells (Figure 6G-H, $P<0.05$ and $P<0.0001$ respectively). We interpret these collective observations to suggest that the increase in mitochondrial mass in TSAd$^{-/-}$ cells is sufficient to sustain metabolic function at baseline and may account for the normal phenotype of Tregs in unmanipulated mice. Nevertheless, our findings indicate that TSAd serves as a link between TCR-dependent signaling in Tregs and mitochondrial function via the translocation of Lck. The additional effects of TSAd on eTreg activation responses and Foxp3 stability are critical to sustain immunoregulation following transplantation.

Discussion

In these studies, we show that the Lck-adaptor protein TSAd elicits cell intrinsic signals in $CD4^+Foxp3^+$ Treg cells that are associated with enhanced activation and immunoregulatory function. Specifically, we find that graft failure is accelerated in $TSAd^{-/-}$ recipients of MHC class II mismatched cardiac transplants and that $TSAd^{-/-}$ recipients are resistant to the graft prolonging effects of costimulatory blockade. Furthermore, in adoptive transfer studies, we show that $TSAd^{-/-}$ Tregs are less efficient than WT Tregs in the suppression of allograft rejection. Untargeted transcriptomic analysis indicates that the major phenotype of $TSAd^{-/-}$ Tregs is a lack of TCR-dependent activation, and mechanistic studies demonstrate that $TSAd^{-/-}$ Tregs lack mitochondrial Lck expression as well as ROS production. Collectively, these findings indicate that TSAd has multiple mechanisms of function in Treg cells. Since mutations in *SH2D2A* (the gene encoding TSAd) are associated with autoimmunity, these observations have broad clinical implications.

Previous studies (3, 5, 14) have demonstrated that TSAd regulates the threshold for TCR-dependent activation in $CD4^+$ Teff cells *in vitro*. Similarly, we find that mitogen-induced activation of naive $TSAd^{-/-}$ $CD4^+$ T cells is attenuated *in vitro* as compared to WT controls. Since TSAd is rapidly induced upon T cell activation, this finding is suggestive that its biological effects are of importance to sustain the continuous activation of effector cells. However, the differentiation of T helper cells is normal in the absence of TSAd (6), and $TSAd^{-/-}$ mice are not immunodeficient (3, 9) and have an improved tumor clearance compared to their wild type littermates (21). In our studies, we find that acute rejection and graft failure is not delayed following fully MHC mismatched transplantation into $TSAd^{-/-}$ mice and alloimmune priming and rejection is enhanced following MHC class II mismatched cardiac transplantation. Thus, despite *in vitro* findings suggesting that TSAd promotes and/or sustains effector responses, we find that alloimmune $CD4^+$ T cell activation is fully functional *in vivo* in the absence of TSAd, suggesting some redundancy in its function.

Nevertheless, a key finding in this study is that the primary biological effect of TSAd relates to its function in $CD4^+Foxp3^+$ Tregs. This finding is consistent with studies demonstrating that $TSAd^{-/-}$ mice, like humans, are prone to the development of autoimmunity (9, 11-13). A major mechanistic observation is the absence of Lck protein expression on mitochondria within $TSAd^{-/-}$ Tregs which is suggestive that TSAd serves (in part) to shuttle Lck from the cytoplasm to the mitochondria of Tregs. It has however been challenging to link this biological response to a generalized defect in immunometabolism. While activation-induced ROS production is absent in Tregs from $TSAd^{-/-}$ mice, we find that the extracellular acidification rate and oxidative phosphorylation is similar to that observed in WT mice. Since there are increased numbers of mitochondria in $TSAd^{-/-}$ Tregs, it is possible that there is some compensation to sustain immunometabolism. However, it is also possible that these effects are independent.

To further define the direct effect(s) of TSAd in Tregs, we performed untargeted transcriptomic profiling of Tregs isolated from TSAd KO and WT mice. These analyses indicate that the major phenotype of KO Tregs is a profound defect in TCR-dependent

activation responses, and there is no major effect of TSAd on mitochondrial or metabolic gene expression. Thus, it is most likely that TSAd functions to elicit eTreg activation responses and these effects are associated with TCR-independent translocation of Lck to mitochondria.

We also questioned whether the effector phenotype (IFN-γ production) of KO Tregs is interrelated with a lack of Lck and ROS production by mitochondria. In pilot studies (not shown), we performed iTreg induction assays in the absence or presence of mitochondrial-specific ROS inhibitors or mitochondrial-specific ROS inducers. Both increased and decreased ROS generation during iTreg induction resulted in lower Foxp3 positivity, but activation responses and IFN-γ expression did not change in the presence of ROS inhibitors or inducers. Thus, we believe that these effects of TSAd are not be linked but are rather related to the generalized effect of TSAd on eTreg activation. Nevertheless, definitive proof will require additional studies, and perhaps the generation of Lck transgenic mice, which are beyond the scope of this report.

Classically, IFN-γ is associated with Teff responses, allograft rejection and $CD4^+$ T helper (Th) 1- and $CD8^+$-mediated immune responses. However, IFN-γ expression has multiple intrinsic and extrinsic functions that are context-dependent in terms of the local tissue microenvironment (36-39). For example, co-expression of the Th1 master transcription factor Tbet in $Foxp3^+$ Tregs is important for controlling Th1 and CD8 effector responses (39), but IFN-γ production by unstable Tregs is reported to break immunological tolerance (36, 40). We observed that $TSAd^{-/-}$ Tregs were efficient in the suppression of $CD4^+$ Teff cell proliferation despite high levels of IFN-γ production. However, analysis of CpG motifs within the TSDR of the *Foxp3* gene demonstrated enhanced methylation, suggesting that the absence of TSAd is associated with reduced lineage stability.

In summary, our findings in this report identify novel cell intrinsic mechanisms whereby TSAd functions to enhance $CD4^+Foxp3^+$ Treg activity. Our observations are most significant for the understanding of immunoregulation following transplantation, especially following treatment with costimulatory blockade (41). In addition, our findings have broad implications (beyond transplantation), since polymorphisms within the *SH2D2A* gene in humans have been linked to autoimmunity.

Supplementary Material

Refer to Web version on PubMed Central for supplementary material.

Acknowledgments

The authors thank Megan Cooper, Kayla MacLeod and Francesca D'Addio (all Boston Children's Hospital, Boston, MA) for technical support and Dr. Gary Visner for supervision of this work within the mouse surgical facility. We also thank Daniel Brown (Beth Israel Deaconess Medical Center, Boston, MA), Dr. Stephen Alexander (The Children's Hospital at Westmead, Sydney, Australia) and Dr. Anne Spurkland (University of Oslo, Norway) for helpful discussions.

Funding: This work was supported by the National Institutes of Health (R21AI92399) and the Casey Lee Ball Foundation (to D.M.B.). J.W. was supported by a fellowship grant from the German Research Foundation (DFG) and a travel grant from the Medical Faculty Mannheim, Heidelberg University, Germany.

Abbreviations:

eTreg	effector/memory Treg
MST	median graft survival
OCR	oxygen consumption rate
ROS	reactive oxygen species
Teff	T effector cell
Treg	T regulatory cell
TCR	T cell receptor
TSAd	T cell specific adaptor protein
TSAd$^{-/-}$	TSAd knockout mouse
TSDR	Treg-Specific Demethylated Region
WT	wildtype

References

1. Spurkland A,Brinchmann JE,Markussen G,Pedeutour F,Munthe E,Lea T,Vartdal F, and Aasheim HC. 1998 Molecular cloning of a T cell-specific adapter protein (TSAd) containing an Src homology (SH) 2 domain and putative SH3 and phosphotyrosine binding sites. J Biol Chem. 273: 4539–46. [PubMed: 9468509]
2. Dai KZ,Vergnaud G,Ando A,Inoko H, and Spurkland A. 2000 The SH2D2A gene encoding the T-cell-specific adapter protein (TSAd) is localized centromeric to the CD1 gene cluster on human Chromosome 1. Immunogenetics. 51: 179–85. [PubMed: 10752626]
3. Rajagopal K,Sommers CL,Decker DC,Mitchell EO,Korthauer U,Sperling AI,Kozak CA,Love PE, and Bluestone JA. 1999 RIBP, a novel Rlk/Txk- and itk-binding adaptor protein that regulates T cell activation. J Exp Med. 190: 1657–68. [PubMed: 10587356]
4. Choi YB,Kim CK, and Yun Y. 1999 Lad, an adapter protein interacting with the SH2 domain of p56lck, is required for T cell activation. J Immunol. 163: 5242–9. [PubMed: 10553045]
5. Lapinski PE,Oliver JA,Bodie JN,Marti F, and King PD. 2009 The T-cell-specific adapter protein family: TSAd, ALX, and SH2D4A/SH2D4B. Immunol Rev. 232: 240–54. [PubMed: 19909368]
6. Perchonock CE,Pajerowski AG,Nguyen C,Shapiro MJ, and Shapiro VS. 2007 The related adaptors, adaptor in lymphocytes of unknown function X and Rlk/Itk-binding protein, have nonredundant functions in lymphocytes. J Immunol. 179: 1768–75. [PubMed: 17641043]
7. Zeng H,Sanyal S, and Mukhopadhyay D. 2001 Tyrosine residues 951 and 1059 of vascular endothelial growth factor receptor-2 (KDR) are essential for vascular permeability factor/vascular endothelial growth factor-induced endothelium migration and proliferation, respectively. J Biol Chem. 276: 32714–9. [PubMed: 11435426]
8. Matsumoto T,Bohman S,Dixelius J,Berge T,Dimberg A,Magnusson P,Wang L,Wikner C,Qi JH,Wernstedt C,Wu J,Bruheim S,Mugishima H,Mukhopadhyay D,Spurkland A, and Claesson-Welsh L. 2005 VEGF receptor-2 Y951 signaling and a role for the adapter molecule TSAd in tumor angiogenesis. EMBO J. 24: 2342–53. [PubMed: 15962004]
9. Drappa J,Kamen LA,Chan E,Georgiev M,Ashany D,Marti F, and King PD. 2003 Impaired T cell death and lupus-like autoimmunity in T cell-specific adapter protein-deficient mice. J Exp Med. 198: 809–21. [PubMed: 12953096]

10. Abrahamsen G,Sundvold-Gjerstad V,Habtamu M,Bogen B, and Spurkland A. 2018 Polarity of CD4+ T cells towards the antigen presenting cell is regulated by the Lck adapter TSAd. Sci Rep. 8: 13319. [PubMed: 30190583]
11. Dai KZ,Harbo HF,Celius EG,Oturai A,Sorensen PS,Ryder LP,Datta P,Svejgaard A,Hillert J,Fredrikson S,Sandberg-Wollheim M,Laaksonen M,Myhr KM,Nyland H,Vartdal F, and Spurkland A. 2001 The T cell regulator gene SH2D2A contributes to the genetic susceptibility of multiple sclerosis. Genes Immun. 2: 263–8. [PubMed: 11528519]
12. Smerdel A,Dai KZ,Lorentzen AR,Flato B,Maslinski S,Thorsby E,Forre O, and Spurkland A. 2004 Genetic association between juvenile rheumatoid arthritis and polymorphism in the SH2D2A gene. Genes Immun. 5: 310–2. [PubMed: 15129233]
13. Lorentzen AR,Smestad C,Lie BA,Oturai AB,Akesson E,Saarela J,Myhr KM,Vartdal F,Celius EG,Sorensen PS,Hillert J,Spurkland A, and Harbo HF. 2008 The SH2D2A gene and susceptibility to multiple sclerosis. J Neuroimmunol. 197: 152–8. [PubMed: 18554728]
14. Marti F,Garcia GG,Lapinski PE,Macgregor JN, and King PD. 2006 Essential role of the T cell-specific adapter protein in the activation of LCK in peripheral T cells. J Exp Med. 203: 281–7. [PubMed: 16446380]
15. Tai X,Cowan M,Feigenbaum L, and Singer A. 2005 CD28 costimulation of developing thymocytes induces Foxp3 expression and regulatory T cell differentiation independently of interleukin 2. Nat Immunol. 6: 152–62. [PubMed: 15640801]
16. Park D,Park I,Lee D,Choi YB,Lee H, and Yun Y. 2007 The adaptor protein Lad associates with the G protein beta subunit and mediates chemokine-dependent T-cell migration. Blood. 109: 5122–8. [PubMed: 17327418]
17. Berge T,Sundvold-Gjerstad V,Granum S,Andersen TC,Holthe GB,Claesson-Welsh L,Andreotti AH,Inngjerdingen M, and Spurkland A. 2010 T cell specific adapter protein (TSAd) interacts with Tec kinase ITK to promote CXCL12 induced migration of human and murine T cells. PLoS One. 5: e9761. [PubMed: 20305788]
18. Sadlack B,Merz H,Schorle H,Schimpl A,Feller AC, and Horak I. 1993 Ulcerative colitis-like disease in mice with a disrupted interleukin-2 gene. Cell. 75: 253–61. [PubMed: 8402910]
19. Malek TR,Yu A,Vincek V,Scibelli P, and Kong L. 2002 CD4 regulatory T cells prevent lethal autoimmunity in IL-2Rbeta-deficient mice. Implications for the nonredundant function of IL-2. Immunity. 17: 167–78. [PubMed: 12196288]
20. Nelson BH 2004 IL-2, regulatory T cells, and tolerance. J Immunol. 172: 3983–8. [PubMed: 15034008]
21. Berge T,Gronningsaeter IH,Lorvik KB,Abrahamsen G,Granum S,Sundvold-Gjerstad V,Corthay A,Bogen B, and Spurkland A. 2012 SH2D2A modulates T cell mediated protection to a B cell derived tumor in transgenic mice. PLoS One. 7: e48239. [PubMed: 23144743]
22. Corry RJ,Winn HJ, and Russell PS. 1973 Primarily vascularized allografts of hearts in mice. The role of H-2D, H-2K, and non-H-2 antigens in rejection. Transplantation. 16: 343–50. [PubMed: 4583148]
23. Wedel J,Bruneau S,Liu K,Kong SW,Sage PT,Sabatini DM,Laplante M, and Briscoe DM. 2018 DEPTOR modulates activation responses in CD4(+) T cells and enhances immunoregulation following transplantation. Am J Transplant. in press.
24. Akimova T,Levine MH,Beier UH, and Hancock WW. 2016 Standardization, Evaluation, and Area-Under-Curve Analysis of Human and Murine Treg Suppressive Function. Methods Mol Biol. 1371: 43–78. [PubMed: 26530794]
25. Wedel J,Bruneau S,Liu K,Kong SW,Sage PT,Sabatini DM,Laplante M, and Briscoe DM. 2019 DEPTOR modulates activation responses in CD4(+) T cells and enhances immunoregulation following transplantation. Am J Transplant. 19: 77–88. [PubMed: 29969188]
26. Kadoki M,Patil A,Thaiss CC,Brooks DJ,Pandey S,Deep D,Alvarez D,Von Andrian UH,Wagers AJ,Nakai K,Mikkelsen TS,Soumillon M, and Chevrier N. 2017 Organism-Level Analysis of Vaccination Reveals Networks of Protection across Tissues. Cell. 171: 398–413 e21. [PubMed: 28942919]

27. Dobin A,Davis CA,Schlesinger F,Drenkow J,Zaleski C,Jha S,Batut P,Chaisson M, and Gingeras TR. 2013 STAR: ultrafast universal RNA-seq aligner. Bioinformatics. 29: 15–21. [PubMed: 23104886]

28. Anders S,Pyl PT, and Huber W. 2015 HTSeq--a Python framework to work with high-throughput sequencing data. Bioinformatics. 31: 166–9. [PubMed: 25260700]

29. Love MI,Huber W, and Anders S. 2014 Moderated estimation of fold change and dispersion for RNA-seq data with DESeq2. Genome Biol. 15: 550. [PubMed: 25516281]

30. Tamayo P,Scanfeld D,Ebert BL,Gillette MA,Roberts CW, and Mesirov JP. 2007 Metagene projection for cross-platform, cross-species characterization of global transcriptional states. Proc Natl Acad Sci U S A. 104: 5959–64. [PubMed: 17389406]

31. Li Y,Li XC,Zheng XX,Wells AD,Turka LA, and Strom TB. 1999 Blocking both signal 1 and signal 2 of T-cell activation prevents apoptosis of alloreactive T cells and induction of peripheral allograft tolerance. Nat Med. 5: 1298–302. [PubMed: 10545997]

32. Nagano H,Mitchell RN,Taylor MK,Hasegawa S,Tilney NL, and Libby P. 1997 Interferon-gamma deficiency prevents coronary arteriosclerosis but not myocardial rejection in transplanted mouse hearts. J Clin Invest. 100: 550–7. [PubMed: 9239401]

33. Schenk S,Kish DD,He C,El-Sawy T,Chiffoleau E,Chen C,Wu Z,Sandner S,Gorbachev AV,Fukamachi K,Heeger PS,Sayegh MH,Turka LA, and Fairchild RL. 2005 Alloreactive T cell responses and acute rejection of single class II MHC-disparate heart allografts are under strict regulation by CD4+ CD25+ T cells. J Immunol. 174: 3741–8. [PubMed: 15749914]

34. Hancock WW,Sayegh MH,Zheng XG,Peach R,Linsley PS, and Turka LA. 1996 Costimulatory function and expression of CD40 ligand, CD80, and CD86 in vascularized murine cardiac allograft rejection. Proc Natl Acad Sci U S A. 93: 13967–72. [PubMed: 8943044]

35. Vahedi S,Chueh FY,Chandran B, and Yu CL. 2015 Lymphocyte-specific protein tyrosine kinase (Lck) interacts with CR6-interacting factor 1 (CRIF1) in mitochondria to repress oxidative phosphorylation. BMC Cancer. 15: 551. [PubMed: 26210498]

36. Overacre-Delgoffe AE,Chikina M,Dadey RE,Yano H,Brunazzi EA,Shayan G,Horne W,Moskovitz JM,Kolls JK,Sander C,Shuai Y,Normolle DP,Kirkwood JM,Ferris RL,Delgoffe GM,Bruno TC,Workman CJ, and Vignali D. a. A.. 2017 Interferon-gamma Drives Treg Fragility to Promote Anti-tumor Immunity. Cell. 169: 1130–1141 e11. [PubMed: 28552348]

37. Koenecke C,Lee CW,Thamm K,Fohse L,Schafferus M,Mittrucker HW,Floess S,Huehn J,Ganser A,Forster R, and Prinz I. 2012 IFN-gamma production by allogeneic Foxp3+ regulatory T cells is essential for preventing experimental graft-versus-host disease. J Immunol. 189: 2890–6. [PubMed: 22869903]

38. Chang CH,Curtis JD,Maggi LB Jr.,Faubert B,Villarino AV,O'sullivan D,Huang SC,Van Der Windt GJ,Blagih J,Qiu J,Weber JD,Pearce EJ,Jones RG, and Pearce EL. 2013 Posttranscriptional control of T cell effector function by aerobic glycolysis. Cell. 153: 1239–51. [PubMed: 23746840]

39. Levine AG,Mendoza A,Hemmers S,Moltedo B,Niec RE,Schizas M,Hoyos BE,Putintseva EV,Chaudhry A,Dikiy S,Fujisawa S,Chudakov DM,Treuting PM, and Rudensky AY. 2017 Stability and function of regulatory T cells expressing the transcription factor T-bet. Nature. 546: 421–425. [PubMed: 28607488]

40. Delgoffe GM,Woo SR,Turnis ME,Gravano DM,Guy C,Overacre AE,Bettini ML,Vogel P,Finkelstein D,Bonnevier J,Workman CJ, and Vignali DA. 2013 Stability and function of regulatory T cells is maintained by a neuropilin-1-semaphorin-4a axis. Nature. 501: 252–6. [PubMed: 23913274]

41. Vincenti F,Larsen C,Durrbach A,Wekerle T,Nashan B,Blancho G,Lang P,Grinyo J,Halloran PF,Solez K,Hagerty D,Levy E,Zhou W,Natarajan K,Charpentier B, and Belatacept Study G. 2005 Costimulation blockade with belatacept in renal transplantation. N Engl J Med. 353: 770–81. [PubMed: 16120857]

Key Points

- TSAd knockout mice mount accelerated rejection responses following transplantation.
- TSAd is a potent regulator of cellular activation in $CD4^+$ Treg cells.
- TSAd knockout $CD4^+$ Tregs fail to shuttle Lck from the cytoplasm to mitochondria.

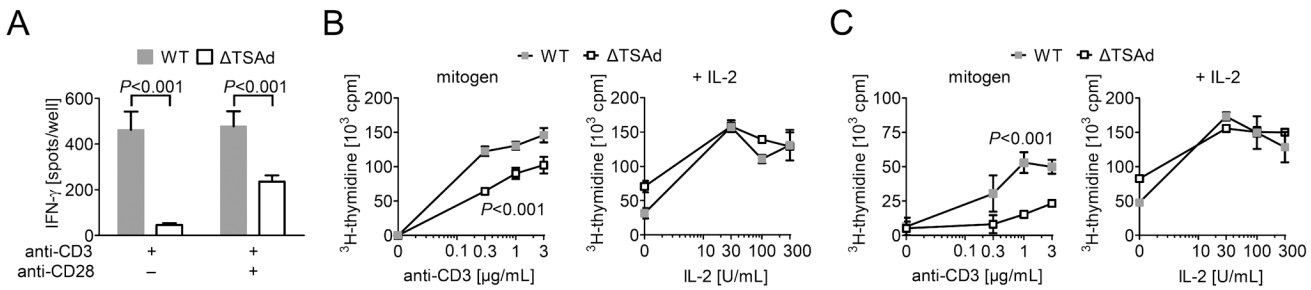

Figure 1. Effect of TSAd on CD4$^+$ T cell activation responses *in vitro*.

(A) Purified CD4$^+$ T cells from WT or TSAd knockout mice (labeled ΔTSAd) were cultured in media with/without plate-bound anti-CD3 and soluble anti-CD28 (1 μg/mL each) for 24 hours, and IFN-γ production was evaluated by ELISPOT. (B) Bead-sorted CD4$^+$CD25$^-$ naive T cells or (C) CD4$^+$CD25^{high} Tregs from WT or TSAd$^{-/-}$ mice were stimulated with increasing concentrations of anti-CD3 alone (0.1-3 μg/mL) or anti-CD3 (1 μg/mL) with increasing concentrations of IL-2. Proliferation was assessed after 72 hours by ^{3}H-thymidine incorporation. Data is expressed as mean counts per minute (CPM) ± SD of a representative experiment performed in triplicate. Each figure is representative of 5 independent experiments. Statistical analyses were performed using the Student's t-test (A) or one-way ANOVA (B-C).

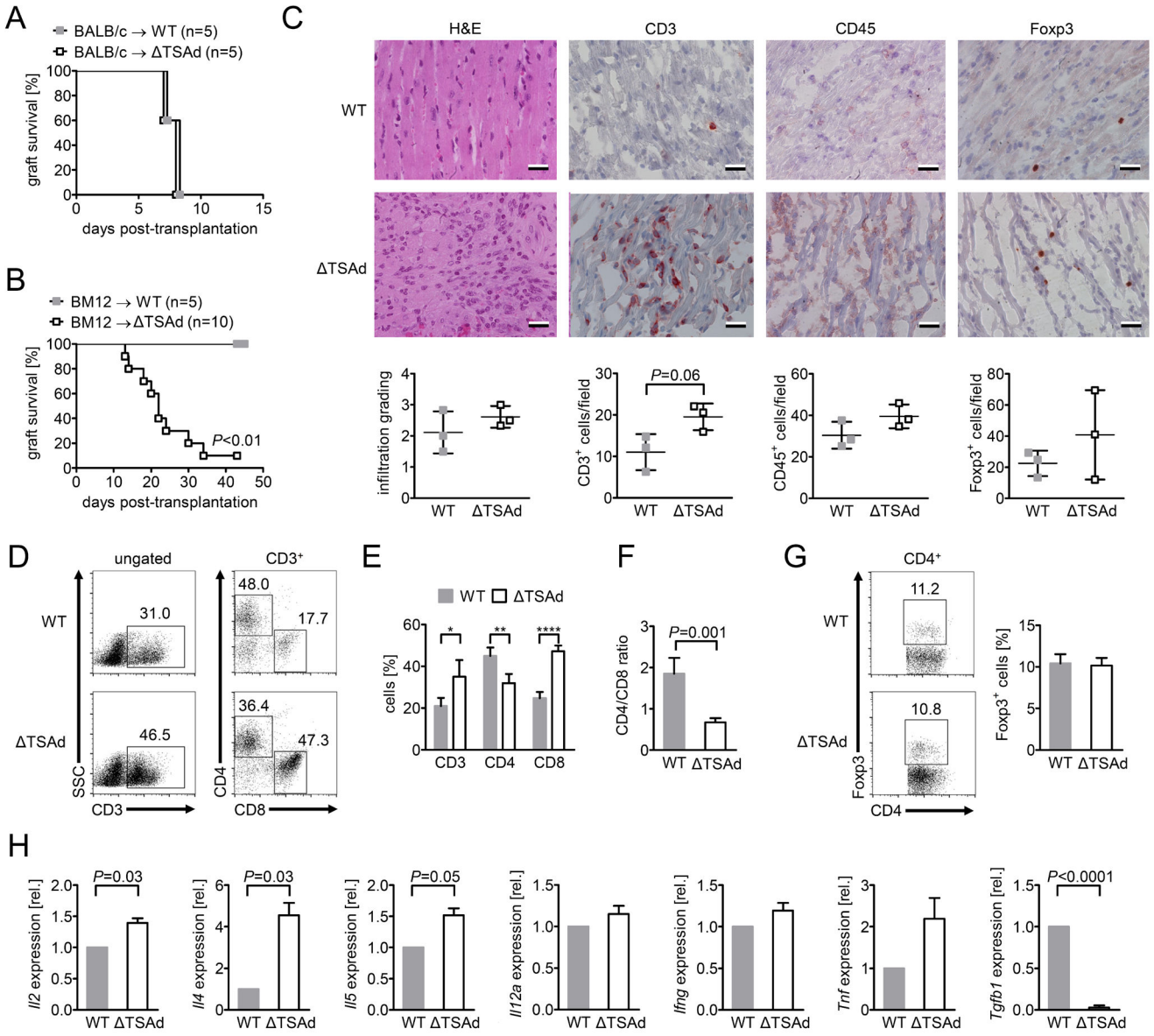

Figure 2. Accelerated rejection of cardiac allografts in TSAd knockout recipient mice.

(A) Graft survival following transplantation of fully MHC mismatched BALB/c hearts into C57BL/6 WT or TSAd knockout (labeled ΔTSAd) recipient mice. (B) Graft survival following transplantation of MHC class II mismatched B6.C-H-2^{bm12} hearts into WT or TSAd knockout recipients (Gehan-Breslow-Wilcoxon test). (C) Histology of B6.C-H-2^{bm12} cardiac allografts harvested on day 18 post-transplantation from WT and TSAd knockout recipients; the upper panels are representative photomicrographs and the lower plots show infiltration as identified by standard grid counting in 3 allografts per condition (Student's t-test). (D-G) Intragraft infiltrates were evaluated on day 18 post-transplantation in allografts harvested from WT or TSAd knockout recipients. *(D)* Representative flow cytometry analysis, *(E)* the mean frequency of CD3$^+$, CD4$^+$ and CD8$^+$ cells, *(F)* the CD4$^+$ to CD8$^+$ ratio ± SD of n=3 animals per group, and *(G),* representative flow cytometry, and bar graphs of the frequency of Foxp3$^+$ cells within the CD4$^+$ population ± SD in n=3 mice/group. (H)

Intragraft cytokine mRNA expression on day 18 post-transplantation by qPCR. Bar graphs represent the relative mRNA expression ± SD of n=3/condition (One sample t-test).

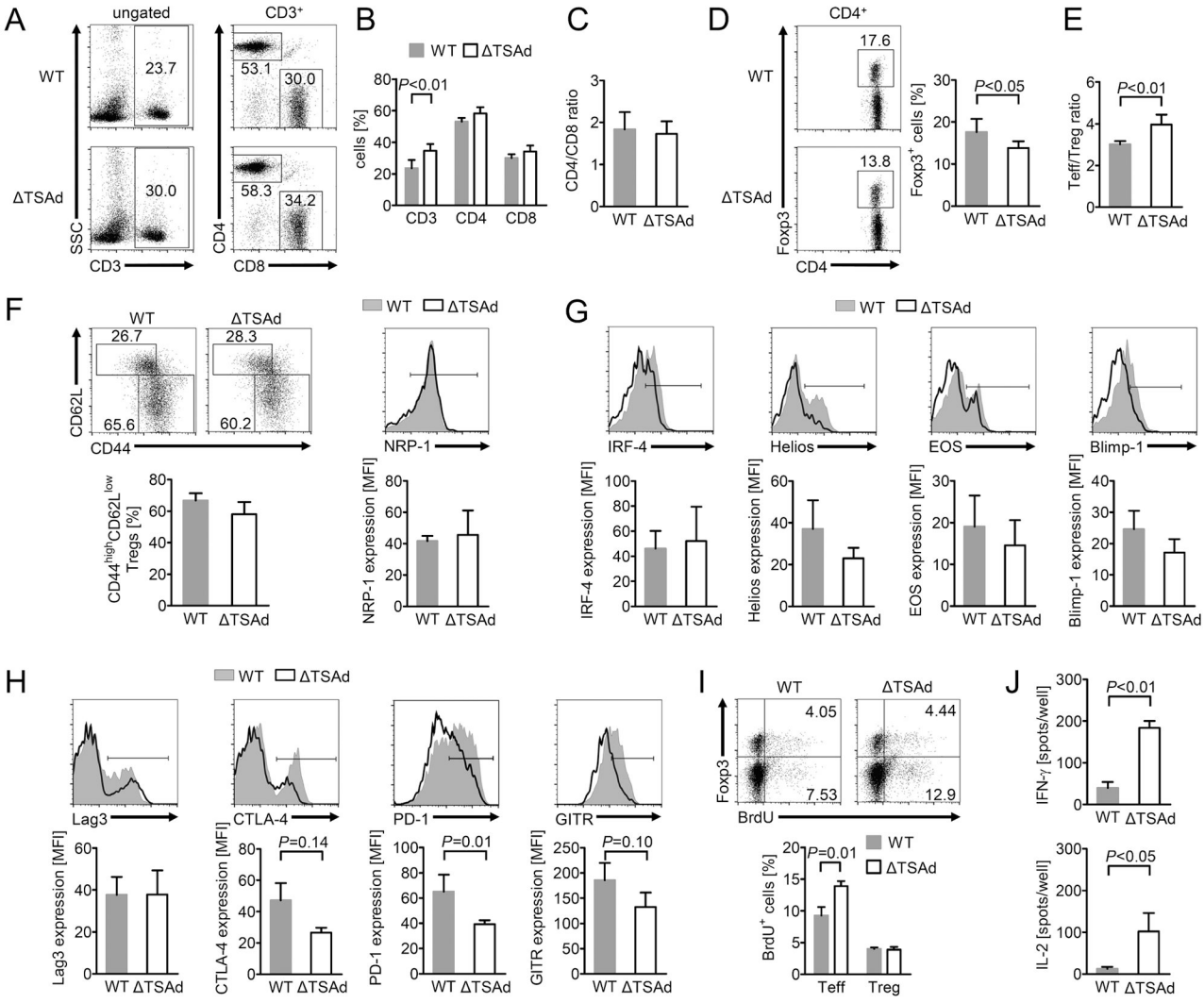

Figure 3. CD4$^+$ T effector/regulatory cell phenotype and expansion in TSAd knockout recipients of cardiac allografts.

Splenocytes from either C57BL/6 WT or TSAd knockout (ΔTSAd) recipients of B6.C-H-2^{bm12} donor allografts were harvested on day 18 post-transplantation and were analyzed by flow cytometry and by ELISPOT. (A) Representative flow cytometry analysis, (B) the mean frequency of CD3$^+$, CD4$^+$ and CD8$^+$ cells, and (C) the CD4$^+$ to CD8$^+$ ratio ± SD of n=4 animals per group. (D) Representative flow cytometry, and bar graphs of the frequency of Foxp3$^+$ cells within the CD4$^+$ population ± SD in n=4 mice. (E) The ratio of CD4$^+$CD44^{high}CD62L^{low} Teff cells to CD4$^+$Foxp3$^+$ Treg ± SD in n=4 mice. (F) The frequency or mean fluorescence intensity (MFI) of CD4$^+$Foxp3$^+$ Treg subsets expressing CD44, CD62L, and NRP-1, (G) the transcription factors IRF-4, Helios, EOS and Blimp-1, and (H) the immunomodulatory proteins Lag3, CTLA4, PD-1 and GITR. (I) On day 15 post-transplantation, recipients were pulsed with BrdU intraperitoneally (every 12 hours for a total of 3 days) and splenocytes were harvested on day 18. A representative dot plot of BrdU incorporation within CD4$^+$Foxp3$^-$ Teffs (lower quadrants) and within CD4$^+$Foxp3$^+$ Tregs (upper quadrants) by flow cytometry. The bar graph illustrates the mean percent of BrdU$^+$

cells ± SD within the Teff or Treg populations in n=4 animals per group. (J) Recipient splenocytes were co-cultured with irradiated (1700 rad) donor antigen presenting cells (B6.C-H-2^{bm12}) in a mixed lymphocyte reaction and allopriming was evaluated by the analysis of IFN-γ (*upper panel*) and IL-2 (*lower panel*) production by ELISPOT. Assays were performed in triplicates and are depicted as mean spots/well ± SD of 6 independent experiments. In each panel, statistical analysis and *P*-values were calculated using the Student's t-test.

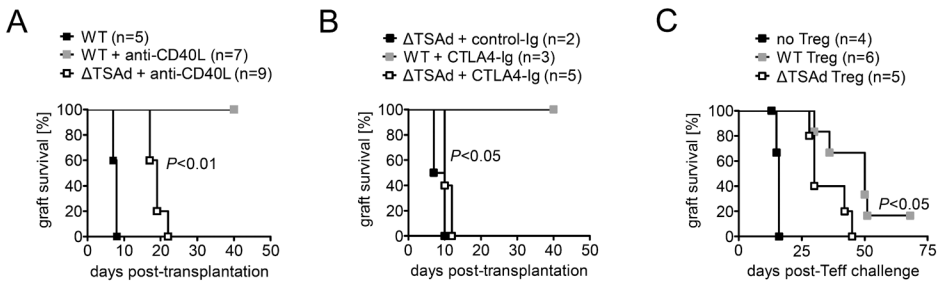

Figure 4. TSAd knockout recipients are resistant to the graft prolonging effects of costimulatory blockade.

Fully MHC mismatched BALB/c hearts were transplanted into WT or TSAd knockout (ΔTSAd) recipients respectively and were treated with (A) anti-CD40L or (B) CTLA4-Ig intraperitoneally on days 0, 2 and 4 post-transplantation. Graft survival was monitored by palpation. Statistics were performed by comparing outcomes in treated ΔTSAd *vs.* treated WT recipients. (C) Fully MHC mismatched BALB/c hearts were transplanted into C57BL/6 *Rag2 Il2rg* double knock-out recipients. On day 2 post-transplantation, recipients received FACS-sorted $CD4^+Foxp3^+$ Treg cells (2×10^5) from either WT or TSAd knockout mice by tail vein injection. On day 18 post-transplantation, recipients were challenged with WT $CD4^+CD25^-$ Teffs (3×10^6 cells) by tail vein injection. Control recipients did not receive Tregs on day 2. Graft survival following Teff transfer was evaluated by palpation. Statistics in A-C were performed using the Gehan-Breslow-Wilcoxon test.

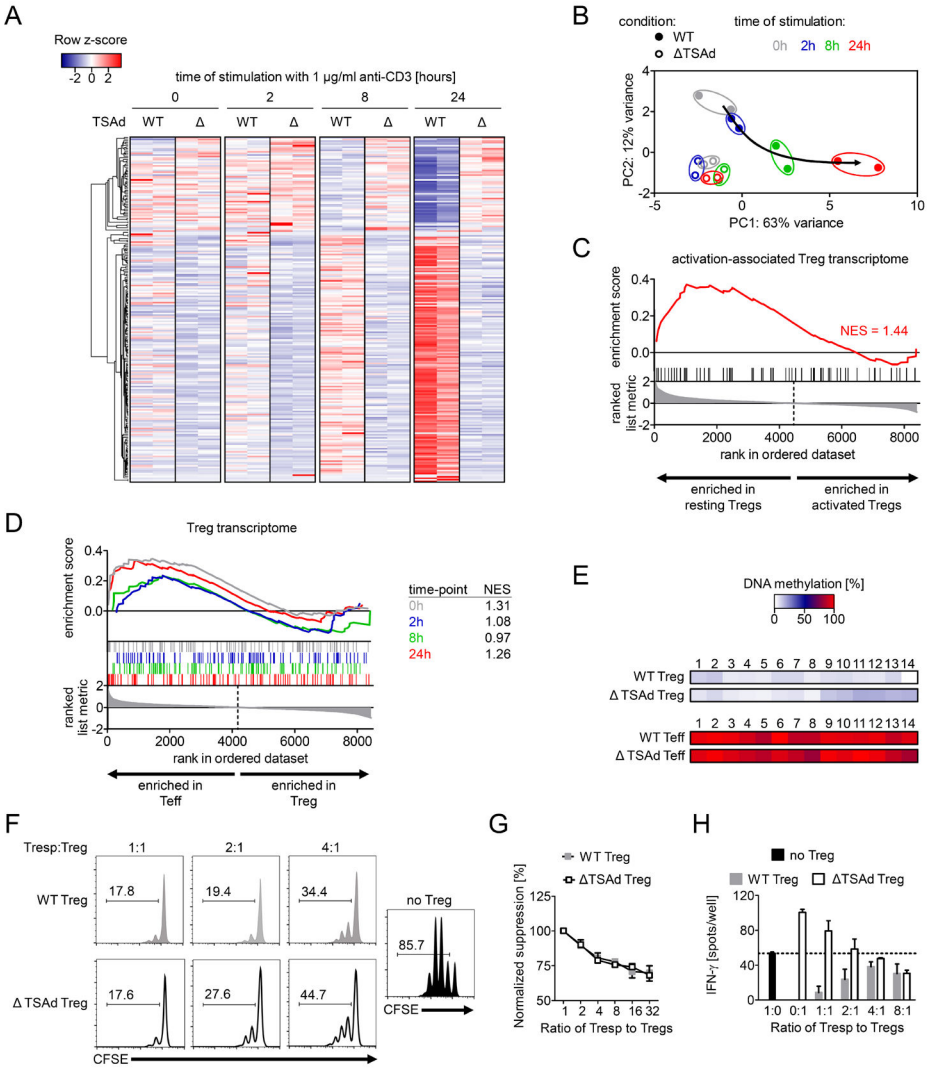

Figure 5. Cell intrinsic function of TSAd in CD4^{+}Foxp3^{+} Tregs.

(A-D) Transcriptomic analysis of FACS-sorted WT and TSAd knockout (Δ) CD4^{+}CD25^{high} Tregs either unactivated or following treatment with anti-CD3 (1 µg/mL) for 2-24 hours. (A) Heatmaps illustrate 222 differentially expressed genes (KO *vs.* WT; *Padj*<0.001 at each time-point). (B) Principal component analysis of differential expressed genes (*Padj*<0.001) following activation of WT (black line/arrow) and TSAd KO Tregs with anti-CD3 for 2-24 hours (each time point is color coded). (C) Gene set enrichment analysis against genes that are upregulated in resting *vs.* activated Tregs (GSE15659: resting Treg *vs.* activated Treg up). *(D)* Gene set enrichment analysis against genes that are upregulated in Tregs *vs.* Teff (each time-point is color coded; GSE20366: TregLP *vs.* TconvLP up). (E) CD4^{+}Foxp3^{+} Tregs and CD4^{+}Foxp3^{-} Teffs were FACS-sorted from the spleens of male WT and TSAd knockout (ΔTSAd) mice, and DNA methylation was assessed by bisulfite-conversion and pyrosequencing. Heat maps represent the mean level of methylation of 14 CpG islands within the TSDR region of the *Foxp3* gene in 2 independent experiments. (F-H) *In vitro* Treg suppression assays were performed using naive CD4^{+} T cells as responders (Tresp) in combination with increasing ratios of FACS-sorted WT or TSAd knockout CD4^{+}CD25^{high}

Tregs. Suppression was assessed by the evaluation of Tresp proliferation (CFSE-dilution in *F-G*) or IFN- γ production (ELISPOT in *H*). (G) Expansion indices were calculated from n=3 independent experiments normalized for Treg suppressive capacity ± SD (Two-way ANOVA; *P*=*n.s.*). (H) The bar graphs illustrating Treg-mediated suppression of responder IFN-γ production ± SD are representative of n=2 experiments performed in triplicate.

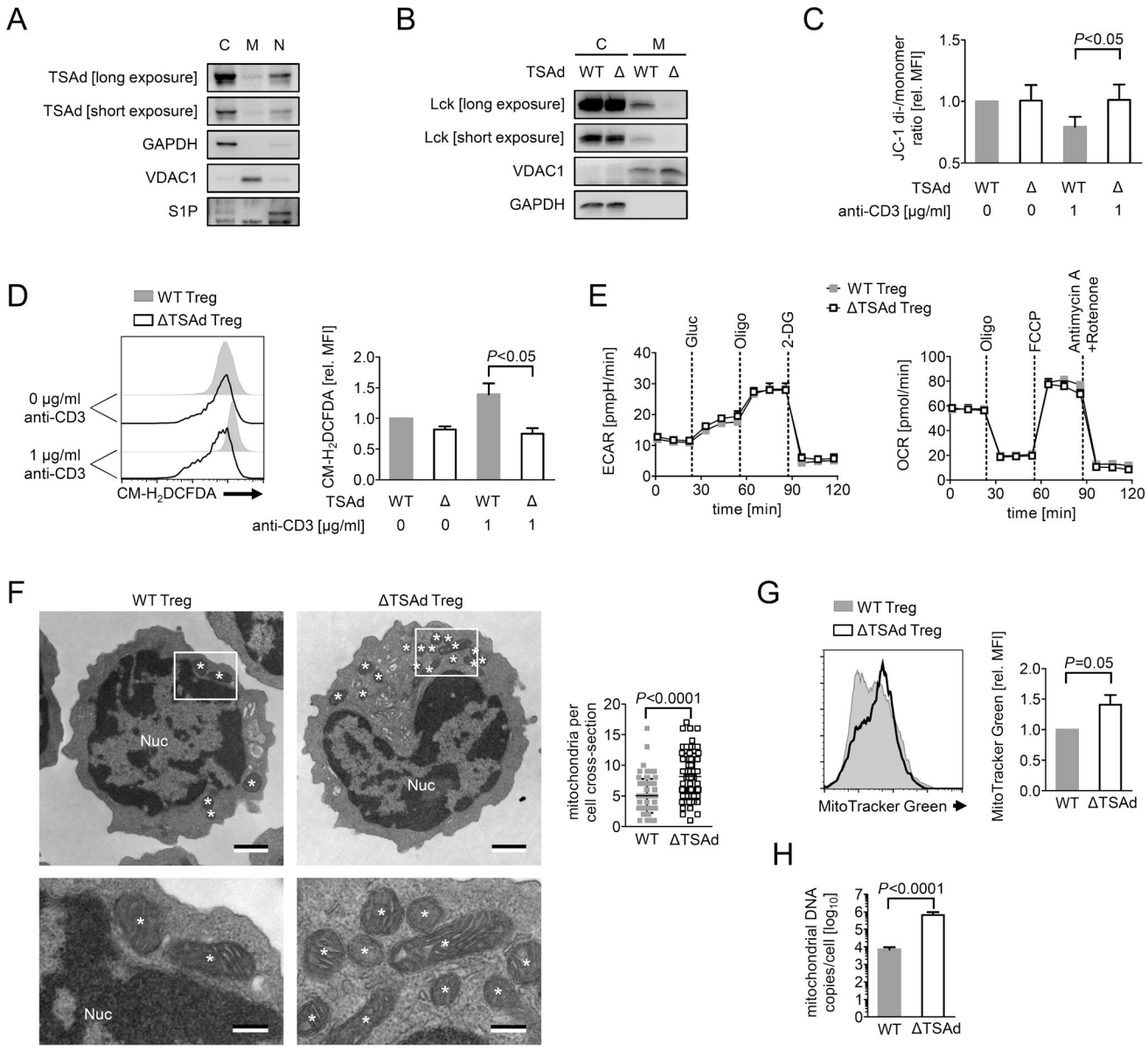

Figure 6. TSAd regulates Lck activity and functional responses within mitochondria of Tregs.

(A) Western blot analysis of cytosolic [C], mitochondrial [M] and nuclear [N] TSAd expression in bead-sorted WT $CD4^+CD25^{high}$ Tregs. Each blot is representative of n=3 independent experiments. (B) Lck expression in cytosolic [C] and mitochondrial [M] extracts from bead-sorted WT or TSAd knockout (ΔTSAd) $CD4^+CD25^{high}$ Tregs by Western blot analysis (representative of n=2 experiments). (C) Mitochondrial membrane potential of WT and TSAd knockout (ΔTSAd) $CD4^+CD25^{high}$ Tregs (gated) as analyzed by flow cytometry using JC-1. The bar graph represents the relative ratio of the mean fluorescence intensity (MFI) of the dimeric to monomeric JC-1 probe ± SD in n=7 experiments (Kruskal-Wallis test). (D) Activation-induced ROS generation by WT or TSAd knockout (ΔTSAd) $CD4^+CD25^{high}$ Tregs (gated) following stimulation with 1 μg/mL anti-CD3 for 30 min. CM-H_2-DCFDA was analyzed by flow cytometry and the bar graph

illustrates the relative MFI ± SD of n=3 independent experiments (Kruskal-Wallis test). (E) Bead-sorted WT and TSAd knockout $CD4^{+}CD25^{high}$ Tregs were stimulated with anti-CD3/anti-CD28 (both at 1 μg/mL) and IL-2 (10 ng/mL) for 24 hours. *Left Panel:* Glycolysis was evaluated by measuring the extracellular acidification rate (ECAR) following the sequential addition of 10 mM glucose (Gluc), 1 μM oligomycin (Oligo) and 100 mM 2-deoxy glucose (2-DG). *Right Panel:* Oxidative phosphorylation was evaluated by measuring the oxygen consumption rate (OCR) following the sequential addition of 2 μM oligomycin (Oligo), 1.5 μM carbonyl cyanide-4-trifluoromethoxy-phenylhydrazone (FCCP), and 1 μM antimycin A and 500 nM rotenone into cultures. One representative of n=2 identical experiments is illustrated (mean ECAR/OCR ± SD of triplicate conditions; Two-way ANOVA, *P=n.s.*). (F) Transmission electron microscopy of bead-sorted $CD4^{+}C25^{high}$ WT and TSAd knockout Tregs. Mitochondria are highlighted with an asterix [*]; the nucleus is labeled [Nuc]. *Upper panel:* Representative cross-sections (1 μm/bar). *Lower Panel:* Box insert from the upper panels at 250 nm/bar. The scatter graph represents the mean number of mitochondria per cell ± SD; one cross section/cell and a total of 40 cells/group (Student's t-test). (G) Mitochondrial mass of WT or TSAd knockout $CD4^{+}CD25^{high}$ Tregs (gated) was analyzed by flow cytometry using MitoTracker Green. Bars represent the relative MFI ± SD of n=6 independent experiments (One-sample t-test). (H) DNA was isolated from bead-sorted WT or TSAd knockout $CD4^{+}CD25^{high}$ Tregs and the mitochondrial mass was evaluated using the ratio of mitochondrial *vs.* nuclear DNA content by qPCR. Bars represent mean mitochondrial DNA copies/cell ± SD of n=3 experiments (Student's t-test).

Table 1.

Primer sequences.

gene	forward primer	reverse primer
Il2	GTGCTCCTTGTCAACAGCG	GGGGAGTTTCAGGTTCCTGTA
Il4	CGTTTGGCACATCCATCTCC	TCATCGGCATTTTGAACGAG
Il5	AAAGAGAAGTGTGGCGAGGAGA	CACCAAGGAACTCTTGCAGGTAA
Il12a	GTCACCTGCCCAACTGCC	TATTCTGCTGCCGTGCTTCC
Ifng	AACGCTACACACTGCATCTTGG	GCCGTGGCAGTAACAGCC
Tnf	CTACTCCCAGGTTCTCTTCAA	GCAGAGAGGGAAAGGTTGACTTTC
Tgfb1	GGTTCATGTCATGGATGGTG	TGAGTGGCTGTCTTTTGACG